

Supplementary information for

Atomic Doping and Light Irradiation Promote Anodic Hydrogen Evolution through Furfural Oxidation on $\text{Cu}_{2+1}\text{O}/\text{Cu}$ Nano-Dendrites

Yuan Xu ^{a,b}, Tao He ^b, Yechan Yin ^b, Liqiu Zhang ^{*b}, Hongxia Shen ^b, Bin Li ^b,

Lichun Liu ^{*a,b}, and Song Bai ^{*a}

^a College of Chemistry and Materials Science, Zhejiang Normal University, Jinhua, Zhejiang Province, 321000, P. R. China

^b College of Biological, Chemical Sciences and Engineering & Nanotechnology Research Institute, Jiaxing University, Jiaxing, Zhejiang Province, 314001, P. R. China

Figures

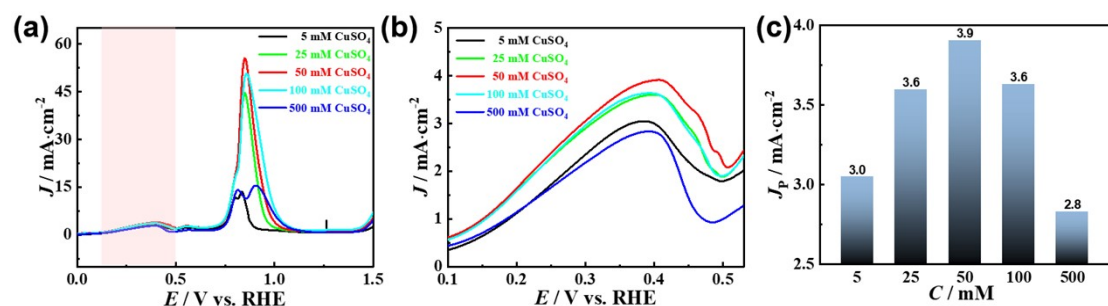


Figure S1. Optimization of CuSO_4 concentration for optimum furfural oxidation. (a) Linear sweep voltammograms of copper nano-dendrites electrodeposited with different concentrations of CuSO_4 . (b) Enlarged LSV curve in shadow region in (a). (c) Diagram of peak current density of furfural oxidation as a function of CuSO_4 concentration.

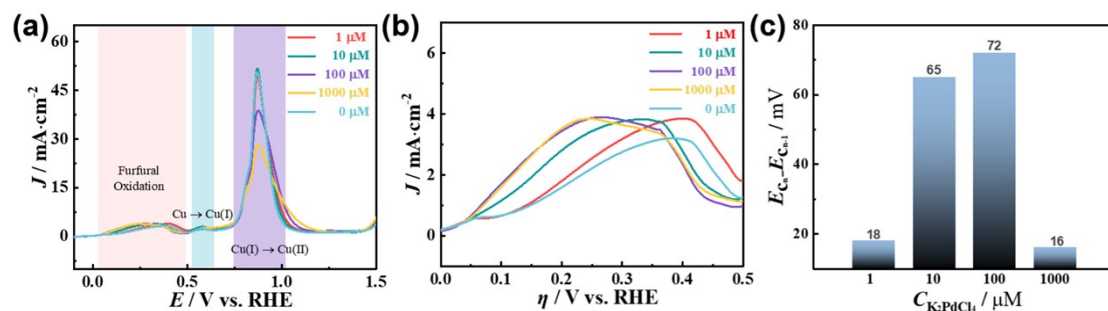


Figure S2. Optimization of K_2PdCl_4 concentration. (a) Linear sweep voltammograms of copper nano-dendrites electrodeposited with different concentrations of K_2PdCl_4 with fixed 50 mM CuSO_4 . (b) Enlarged LSV curve in the 0-0.5V region in (a). (c) Diagram of peak potential shift of furfural oxidation as a function of K_2PdCl_4 concentration.

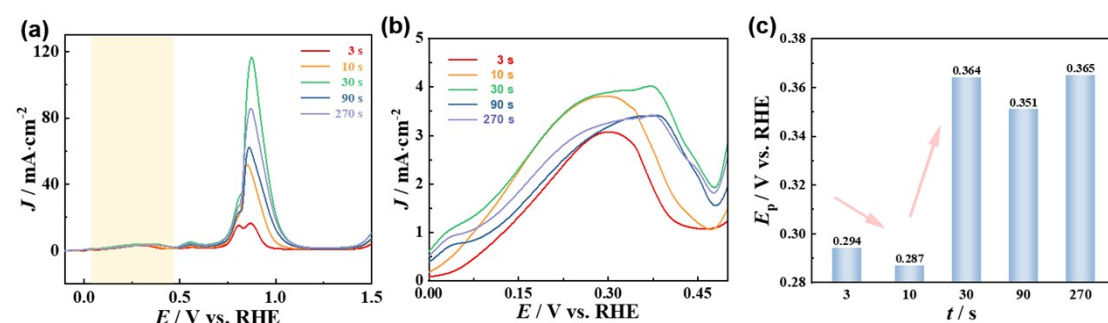


Figure S3. Optimization of deposition time. (a) Linear sweep voltammograms of copper nano-dendrites electrodeposited at different times using electrolyte solution containing 100 μM of K_2PdCl_4 with fixed 50 mM of CuSO_4 . (b) Enlarged LSV curve in the 0-0.5V region in (a) showing furfural oxidation behavior. (c) Diagram of peak potential of furfural oxidation as a function of K_2PdCl_4 concentration.

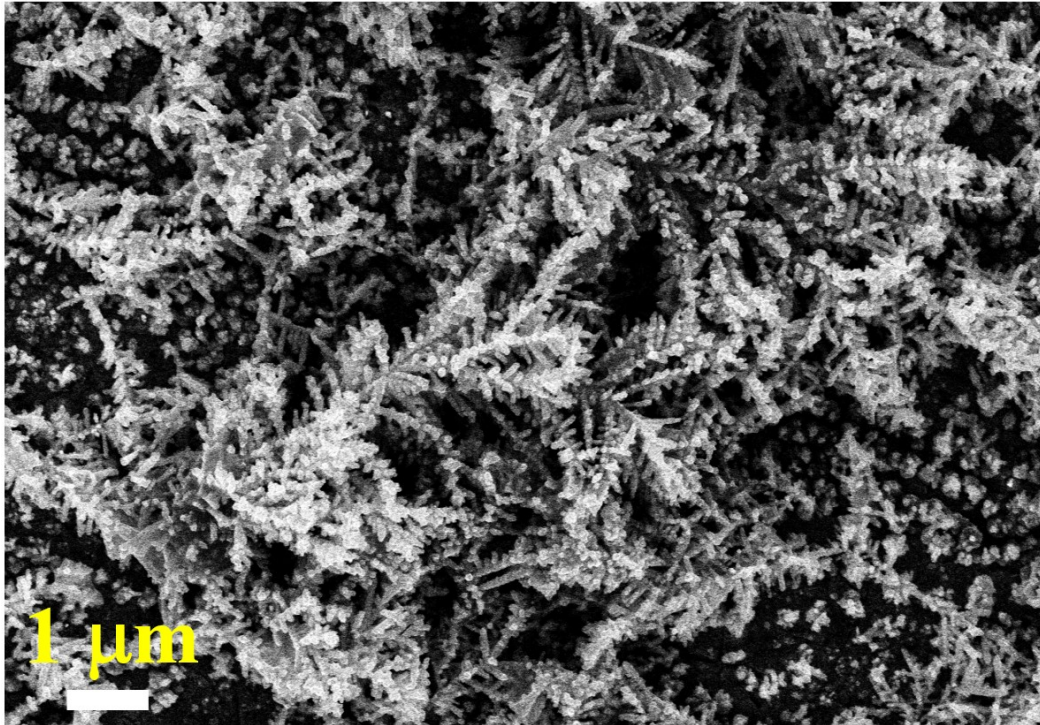


Figure S4. SEM image of a typical electrodeposit using the electrodeposition technique.

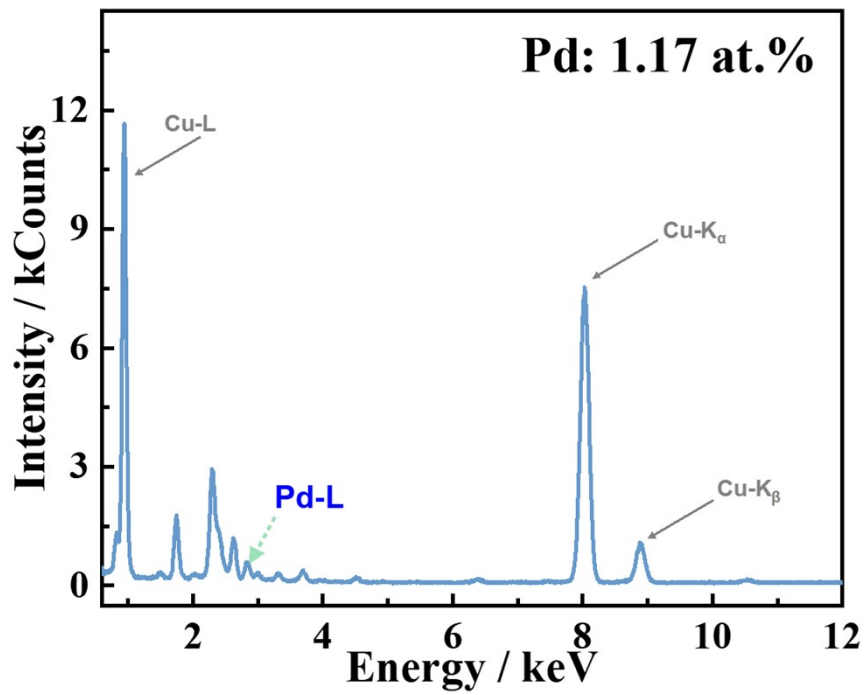


Figure S5. Energy dispersive spectrum of Pd@Cu₂₊₁O/Cu NDs. Inset: ICP/MS result.

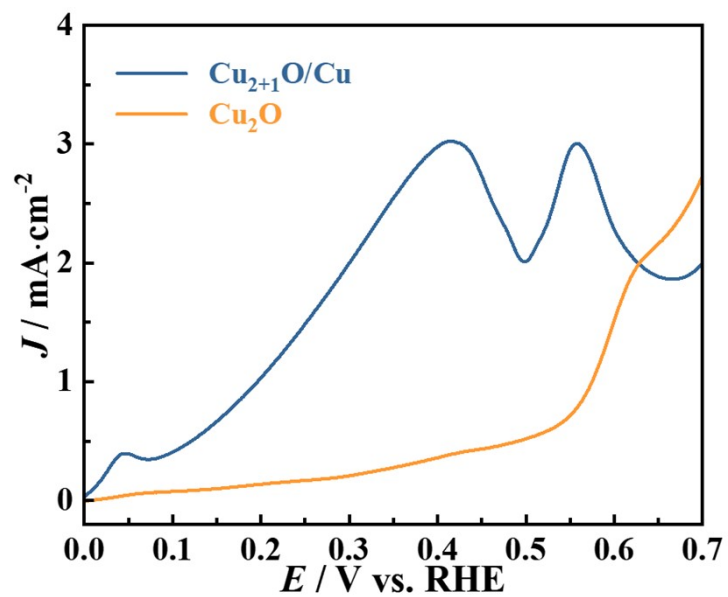


Figure S6. Comparison on current densities of furfural oxidation on $\text{Cu}_{2+1}\text{O}/\text{Cu}$ and Cu_2O . Cu_2O was prepared by 2h electrooxidation by fixing potential at 0.55 V vs RHE in 1 M KOH.

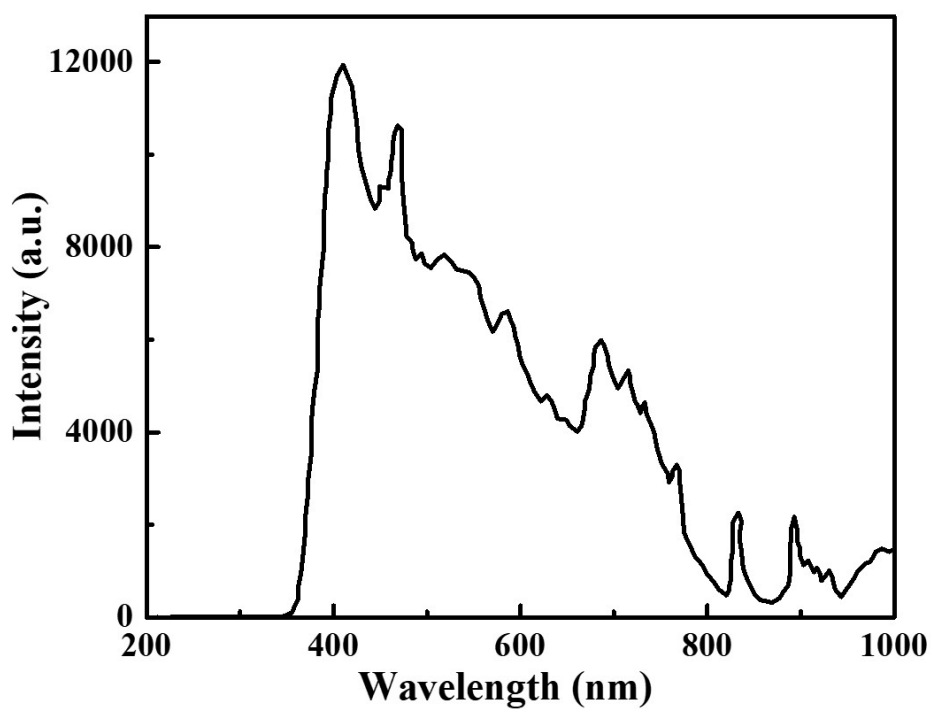


Figure S7. The optical spectra of visible light produced by the light source.

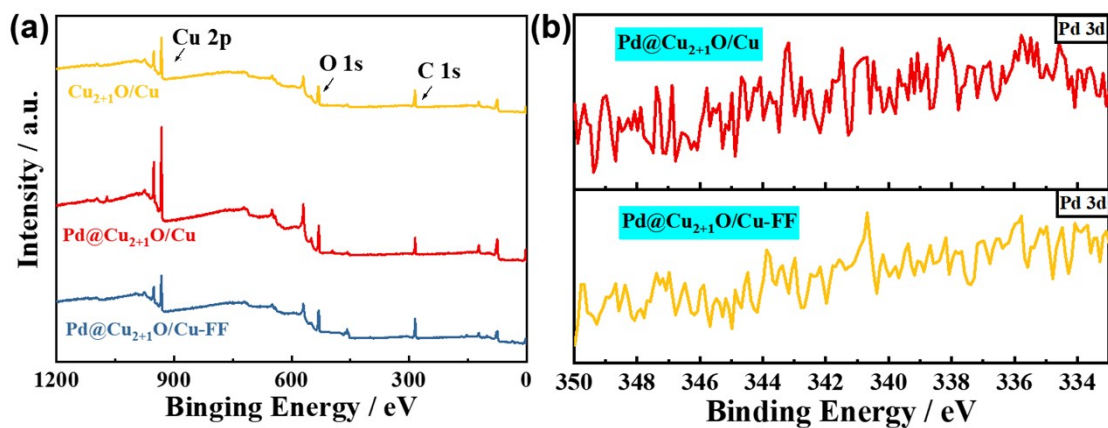


Figure S8. (a) Full spectra of XPS for $\text{Cu}_{2+1}\text{O}/\text{Cu}$ and $\text{Pd}@\text{Cu}_{2+1}\text{O}/\text{Cu}$ NDs. (b) XPS spectra of Pd 3d for $\text{Cu}_{2+1}\text{O}/\text{Cu}$ and $\text{Pd}@\text{Cu}_{2+1}\text{O}/\text{Cu}$ NDs.

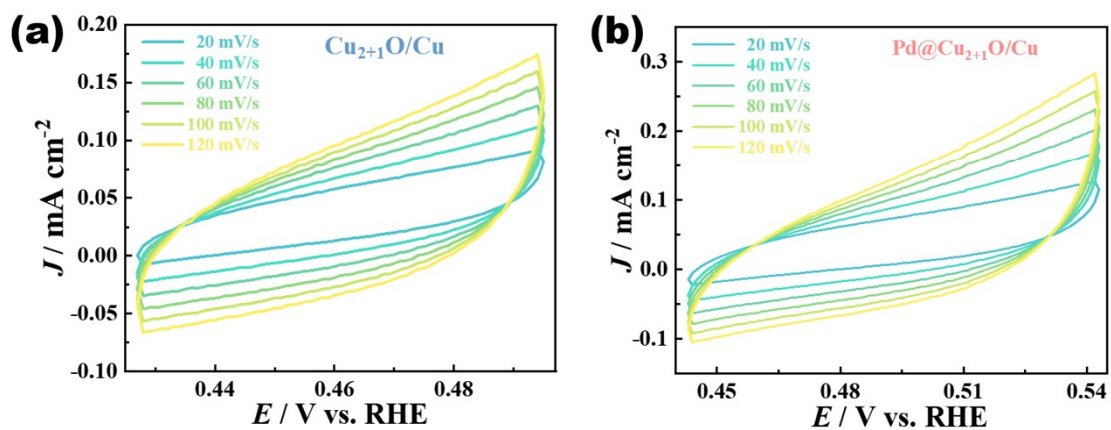


Figure S9. Cyclic voltammograms at different scan rates for $\text{Cu}_{2+1}\text{O}/\text{Cu}$ (a) and $\text{Pd}@\text{Cu}_{2+1}\text{O}/\text{Cu}$ NDs (b). Potential range is set by $\text{OCP} \pm 50 \text{ mV}$.

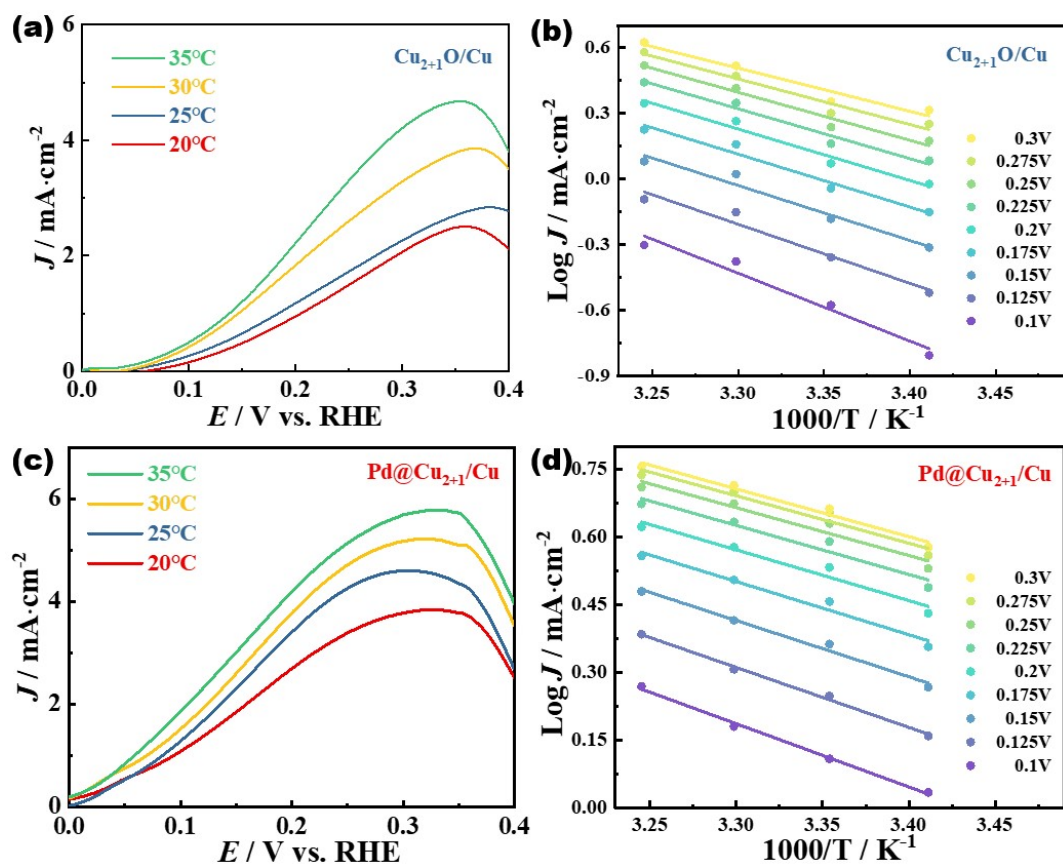


Figure S10. LSV curves of $\text{Cu}_{2+1}\text{O}/\text{Cu}$ (a) and $\text{Pd}@Cu_{2+1}\text{O}/\text{Cu}$ (c) at different temperatures in 1 M KOH electrolyte containing 50 mM furfural; and their corresponding $\log_{10} j \sim 1000/T$ curves for $\text{Cu}_{2+1}\text{O}/\text{Cu}$ (b), and $\text{Pd}@Cu_{2+1}\text{O}/\text{Cu}$ (d).